

**THEORETICAL STUDIES OF THE OUTER ENVELOPES
OF YOUNG STELLAR OBJECTS**

Grant NAGW-511

Semiannual Progress Report No. 16 and Final Report

For the period 1 April 1991 through 30 September 1991
For the period 1 October 1983 through 31 December 1991

Principal Investigator

Dr. Lee Hartmann

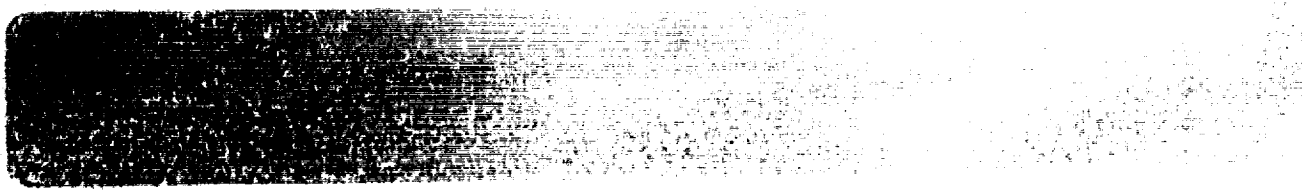
March 1992

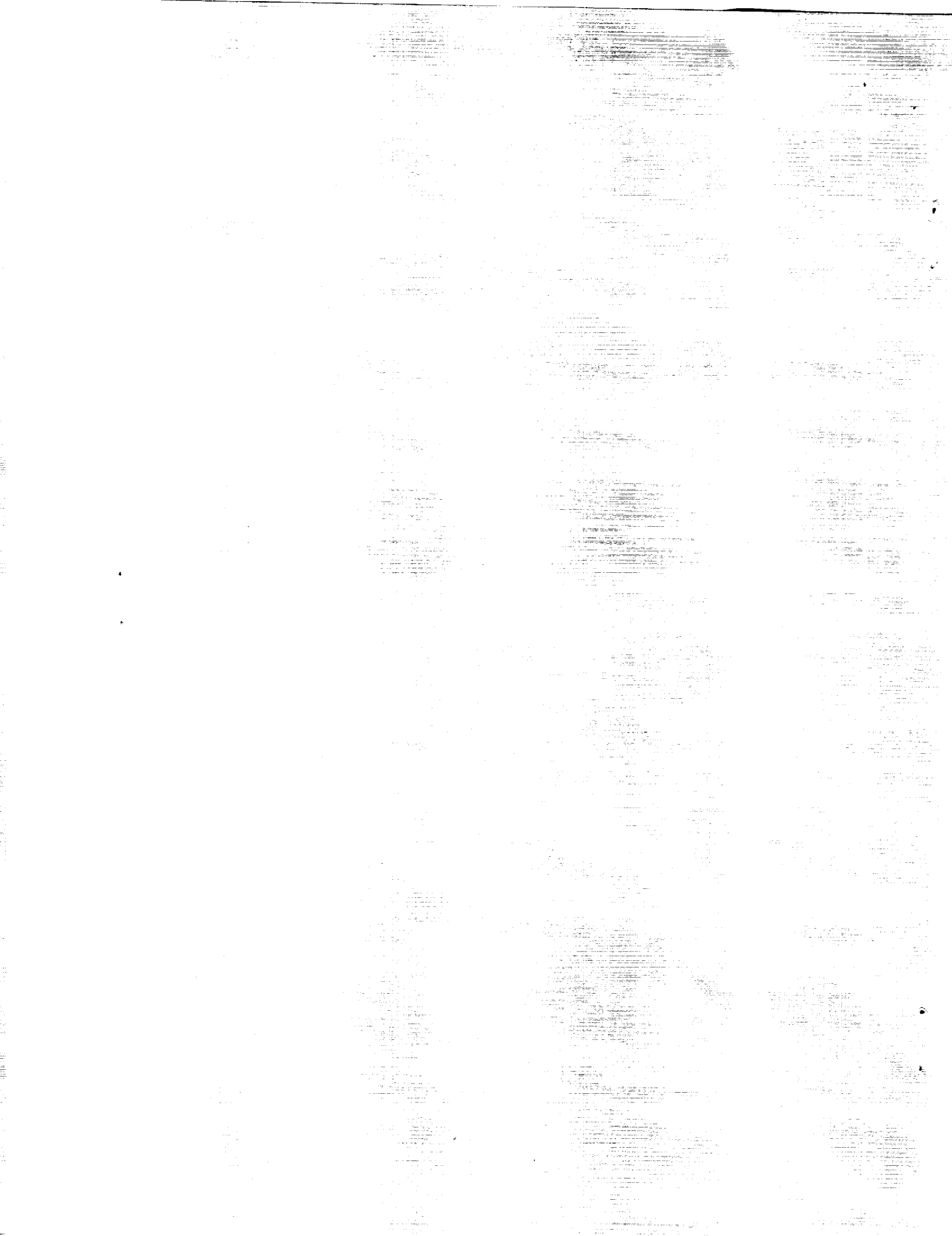
Prepared for
National Aeronautics and Space Administration
Washington, D.C. 20546

Smithsonian Institution
Astrophysical Observatory
Cambridge, Massachusetts 02138

The Smithsonian Astrophysical Observatory
is a member of the
Harvard-Smithsonian Center for Astrophysics

The NASA Technical Officer for this grant is Dr. R. V. Stachnik - Code EZ, Headquarters, National Aeronautics and Space Administration, Washington, D.C. 20546.





Semiannual Report for NAGW-511

Dust Scattering Models for T Tauri Disks and Envelopes

With the Monte Carlo code developed by B. Whitney and L. Hartmann, we have computed a series of models of scattering in disks around young stellar objects. The code calculates scattering by dust, including polarization, in arbitrary geometries. By computing model images, we found that disks, by themselves, around young stellar objects would be very difficult to detect with present-day imaging techniques. The canonical geometrically thin accretion disk illuminated by a central T Tauri star scatters very little light at distances of many AU from the star. An optically thick disk which has a "flaring" surface may be observable, especially if viewed nearly edge-on so that the stellar source becomes occulted. Such a surface provides more solid angle to intercept (and scatter) stellar light. Example images are shown in Figure 1 of a flared disk illuminated by a star at the center. The disk is 500 AU in radius and the scale height of the disk increases with radius as $h \sim r^{9/8}$. The contours show the light distribution at V (5500 Å), normalized to the peak flux in a pixel of the image. Each contour level increases by a factor of 2. The minimum contours for each image are, going in increasing μ , 0.01, 1×10^{-4} , 5×10^{-5} , and 5×10^{-5} . The straight lines indicate polarization vectors, with the position angle shown by the orientation of the lines and the length of the lines showing the magnitude of the polarization. The total polarization is shown with each image. The position angle is oriented perpendicular to the disk plane. Only the image in which the central source is occulted ($\mu = 0.1$) shows a high amount of relative flux, and high polarization. The other images have such high contrast between the stellar flux and diffuse flux that measurement would be difficult.

In comparing these images to observations of young stellar objects which show diffuse structure, we find little resemblance. Objects such as HL Tau and L1551 IRS 5 show a bowl-like structure at infrared wavelengths, which has been attributed to a flared disk by several authors (Monin *et al.* 1989, Strom *et al.* 1985). These objects also have high polarization with position angle oriented parallel to the presumed disk plane (perpendicular to the jet directions). The high polarization indicates that the central source is obscured, and the position angle indicates that significant material lies above the disk plane. A flared disk system will only give high polarization when viewed edge-on, and the position angle is always oriented perpendicular to the disk plane.

This suggests that an envelope, perhaps the remnant infalling envelope, must be present to scatter more stellar light than a disk can, and obscure the star at many inclinations. We have computed a grid of models of scattering in a disk+envelope system. We use the envelope density structure of a rotationally flattened cloud in free fall (Terebey, Shu and Cassen 1984, Cassen and Moosman 1981). The addition of angular

momentum to the infall solution causes material to fall onto a disk thereby decreasing the optical depth through the envelope to the star. This allows scattered light to be seen even in embedded protostars assuming the usual values of infall rate and rotation rates for the Taurus molecular cloud. Wind-blown cavities allow stellar light to escape more easily and scatter off the walls of the envelope. This is illustrated in Figure 2, which shows an object surrounded by an envelope with bipolar holes. The hole shape was chosen to be a streamline of the material which falls in from an angle with cosine $\mu_0 = 0.87$. We assume a wind has blown out a hole within this angle and particles continue to fall in on streamlines beyond this angle. At large distances the streamline shape is radial, as can be seen in Figure 2. The images are shown at an inclination of $\mu = 0.6$. The left panels are models run with forward-scattering high-albedo dust, typical properties at visual wavelengths. The right panels have low-albedo, Rayleigh scattering dust more likely in the infrared. The opacities vary by a factor of 10 going from top to bottom, as shown by the optical depth variation. The optical depth through the envelope is proportional to $\kappa/(250\text{cm}^2/\text{gm})\dot{M}/(2 \times 10^{-6}\text{M}_\odot\text{yr}^{-1})(r_c/(100\text{AU}))^{-1/2}$, where r_c is the centrifugal radius determined by the angular momentum of the original cloud at the furthest radius from which the material collapsed. Thus the sequence in images from top to bottom can be thought of as a sequence in wavelength (opacity) going from optical to IR, infall rate, disk size, or combinations of these.

The top panels have an optical depth of 9.1 through the envelope yet a significant amount of scattered light can be seen. The polarization maps resemble observations of many young stellar objects (e.g. Gledhill and Scarrott 1989; Draper, Warren-Smith and Scarrott 1985; Scarrott, Draper and Warren-Smith 1989), especially the elliptical pattern of the vectors at the higher optical depths. The total system polarization is aligned parallel to the disk at high opacity and perpendicular at low. This position angle rotation is a feature observed in some objects such as T Tau. Note that the polarization can be large even in very optically thick envelopes, if it has wind-blown holes. A typical dust albedo of $\omega \leq 0.5$ insures that most photons are singly scattered, and a hole allows light to scatter mostly in the polar regions. Such an asymmetric geometry for scattering leads to very high polarization. Thus, large polarization should not be interpreted as due to single scattering in optically thin envelopes. In fact, at low optical depths, the envelope becomes more symmetric, the star less obscured, and the total system polarization actually decreases (lower panel in Figure 2).

The longer wavelength images appear bowlshaped. This is not due to scattering in the disk but scattering in the envelope. The objects that typically show these "disk"-like structures are usually the same ones with far-IR excesses, fit by accretion disk models with temperature-radius relations which are too flat to be explained with normal accretion. The spectral energy distributions of these objects should perhaps be re-interpreted in the context of envelopes instead of accretion disks.

FU Orionis Disk Winds

The discovery of powerful bipolar outflows from pre-main sequence objects indicates that mass loss plays an important role in star formation (Lada 1985; Shu, Lizano, & Adams 1987; Edwards, Ray, & Mundt 1991; and references therein). Bipolar outflows appear to be quite common in the earliest stages of star formation (Terebey, Vogel, & Myers 1989) and can easily disperse the material surrounding the central source. In certain cases, long and remarkably thin optical “jets” of material emanate from young objects (Reipurth 1989). The kinetic energy carried by these jets often amounts to $\gtrsim 10\%$ of the total system luminosity (Lada 1985).

The most popular theories for producing bipolar flows or jets from young stars tap the energy liberated as material accretes through a circumstellar disk onto the central star (Adams, Lada, & Shu 1987; Kenyon & Hartmann 1987; Bertout, Basri, & Bouvier 1988; Basri and Bertout 1989). In these theories, high velocity gas is ejected either from a rapidly-rotating central star (Hartmann & MacGregor 1982; Shu *et al.* 1988; Ruden *et al.* 1990) or from an accretion disk (Pudritz & Norman 1983; Königl 1989; Pringle 1989; Pelletier & Pudritz 1991). In both types of models, material is flung outward along strong magnetic field lines anchored in the star or in the disk. The rotating magnetic field ultimately collimates the flow into bipolar jets (e.g., Blandford and Payne 1982).

The source of the mass loss from young stars is controversial, because many bipolar flow sources are heavily reddened and therefore not directly observable. However, optical observations can be employed to study the wind acceleration region in several young FU Orionis variables that have powerful outflows and are not strongly reddened (Reipurth 1989, 1990; Hartmann *et al.* 1991). FU Orionis objects are thought to be protostellar disks undergoing rapid mass accretion at rates of $\dot{M}_{\text{acc}} \gtrsim 10^{-4} M_{\odot} \text{yr}^{-1}$ (Hartmann & Kenyon 1985; Hartmann *et al.* 1991), and thus provide good laboratories for studying the connection between protostellar disk accretion and mass loss. The prototype of the class, FU Ori, has a strong wind (Herbig 1966; Bastian & Mundt 1985), with a mass loss rate $\sim 10^{-5} M_{\odot} \text{yr}^{-1}$ (Crowell *et al.* 1987), and a terminal wind velocity $v \sim -300 \text{ km s}^{-1}$ detected in the strong H α line.

If FU Ori has a disk wind, spectral lines of different strengths should display different profiles. Strong lines, formed in the outermost disk atmosphere, should exhibit strongly blueshifted absorption components. Conversely, weak lines formed in deeper, denser disk layers should exhibit profiles in which rotation dominates, since by mass conservation the expansion velocities will be small in dense regions. The line profiles should vary continuously as the line opacity increases, so that lines of intermediate strength should exhibit intermediate (small) blueshifts. Observations provide qualitative support for this picture; strong Fe II lines exhibit “shell” absorption at velocities of ~ -80 to -50 km s^{-1} (Herbig 1966; Petrov & Herbig 1992), while weak lines are symmetric and double-peaked. In addition, moderately strong photospheric lines in the blue spectral

region are asymmetric, and show blueshifts of $\sim -10 \text{ km s}^{-1}$ (Hartmann & Kenyon 1985, 1987a,b; Kenyon *et al.* 1988 = KHH; Welty *et al.* 1991). Although this behavior is consistent with the disk wind hypothesis, no quantitative model for the lines has yet been constructed.

We have submitted a manuscript entitled “Mass Loss from Protostellar Accretion Disks. I. The Accelerating Wind of FU Orionis” by Calvet, Hartmann, and Kenyon. In this paper we present evidence that the wind of the pre-main sequence object FU Orionis arises from the surface of the luminous protostellar accretion disk. A disk wind model calculated assuming radiative equilibrium explains the differential behavior of the observed asymmetric absorption line profiles. The model predicts that strong lines should be asymmetric and blueshifted, while weak lines should be symmetric and double-peaked due to disk rotation, in agreement with observations.

We considered a viscous, geometrically thin, optically thick accretion disk with constant mass accretion rate \dot{M}_{acc} surrounding a star with mass M and radius R_i . The reference height H measured in the direction outward from the disk midplane (z) varies with cylindrical radius r as $H = H_o (r/R_i)^{9/8}$. We take $H_o = 0.1 R_i$, which is consistent with some theoretical models of FU Ori objects (Clarke *et al.* 1990).

Our radiative transfer solutions assume that spectral lines form close to the (geometrically thin) disk, so we neglect radial energy transport and adopt a plane-parallel geometry. We first calculate a plane-parallel model atmosphere at each disk annulus assuming hydrostatic equilibrium, as discussed in detail by Calvet *et al.* (1991b). This model neglects viscous dissipation within the photosphere, so radiative equilibrium holds and viscous energy generation in deeper disk layers determines the surface radiative flux. The constant radiative flux through the optically thick disk atmosphere can be characterized by an effective temperature

$$T_{\text{eff}} = \left[\frac{3GM\dot{M}_{\text{acc}}}{4\pi\sigma r^3} \left(1 - \left(\frac{R_i}{r} \right)^{1/2} \right) \right]^{1/4} \quad (1)$$

(Shakura & Sunyaev 1973; Lynden-Bell & Pringle 1974). The vertical temperature structure is calculated using the grey atmosphere approximation in the Eddington approximation for a Rosseland mean optical depth τ . To calculate the structure of the atmosphere at each radius r we assume that the reference height H corresponds to the level $\tau = 2/3$, and solve by iteration the system of equations

$$\frac{dp}{d\tau} = \frac{g(z)}{\chi_{\text{Ross}}}, \quad (2)$$

$$\frac{dz}{d\tau} = -\frac{1}{\chi_{\text{Ross}} \rho}, \quad (3)$$

where the height-dependent gravity is given by

$$g(z) = \frac{GM(H+z)}{[r^2 + (z+H)^2]^{3/2}}. \quad (4)$$

Here χ_{Ross} is the Rosseland mean opacity, ρ is the density, and z is the height of the atmosphere above the $\tau = 2/3$ level. Atomic and molecular populations are calculated assuming LTE.

Having calculated a radiative equilibrium atmosphere assuming hydrostatic equilibrium throughout, we then modify the structure by introducing the disk wind. For simplicity we assume that material flows away from the disk midplane in the vertical (z) direction at a velocity v . We further assume that the mass loss per unit area ρv at cylindrical disk radius r varies as

$$(\rho v)_r = (\rho v)_0 (r/R_i)^{-a_1} = \frac{\dot{M}_0}{4\pi R_i^2} (r/R_i)^{-a_1}, \quad (5)$$

where \dot{M}_0 and a_1 are constant input parameters. At each r we define a level z_s from the relation

$$(\rho v)_r(z_s) = \rho_s c_s, \quad (6)$$

where ρ_s is the density given by the hydrostatic equilibrium solution and c_s is the adiabatic sound speed ($\gamma = 5/3$). We assume that the flow is smoothly accelerating outwards; therefore the flow is subsonic for $z < z_s$ and is supersonic for $z > z_s$. In the subsonic region, below z_s , we assume that the density structure is given by hydrostatic equilibrium, which should be true asymptotically proceeding toward the disk midplane. In the supersonic region, above z_s , we adopt a velocity law $v(r, z)$ and compute the density from mass conservation for steady flow.

The velocity structure of a rotating hydromagnetic wind depends in detail on several parameters including the magnetic field strength and structure that are not currently predictable from first principles (Blandford & Payne 1982; Lovelace *et al.* 1987). The flow velocities of the spherically self-similar models of Blandford and Payne (1982) scale as $V(z/r) \propto V_{Kep}(r_0)$, where V_{Kep} is the Keplerian velocity where the field line enters the disk at $r = r_0$. We therefore adopt a simple parameterization of the vertical velocity structure and assume that the wind velocity increases linearly with distance above z_s :

$$v(r, z) = \Gamma V_{Kep}(r) \times (z - z_s)/r + c_s(z_s), \quad z > z_s. \quad (7)$$

The density in the supersonic region is then given by

$$\rho(r, z) = \frac{(\rho v)_r}{v(1 + 1.58(z + H)/r)}, \quad (8)$$

with v determined by equation (7), and z_{max} is an arbitrary cutoff chosen so that $v(z_{max}) = 100 \text{ km s}^{-1}$. (The factor $(1 + 1.58(z + H)/r)$ represents a departure from mass conservation in cylindrical geometry, and is motivated by the divergence of field lines in the standard model of Blandford & Payne (1982). The difference from cylindrical mass conservation only becomes important when $z \approx r$, where our approximation of plane-parallel geometry breaks down anyway.)

With fixed $\rho(z)$, the new Rosseland optical depth and temperature scales are determined at each z by integrating inward from z_{max} ,

$$\tau(z) = \tau(z - \Delta z) + \chi(\rho(z), T(z))\Delta z. \quad (9)$$

Using the grey Eddington expression for the temperature,

$$T(\tau)^4 = 3/4 T_{eff}^4 (\tau(z) + 2/3), \quad (10)$$

equation (9) can be solved as an implicit equation for $\tau(z)$. Finally, the pressure is calculated from the equation of state, interpolating at given density and temperature in pre-calculated tables of mean molecular weight.

The introduction of the wind, with finite continuum optical depth, increases the total optical depth in the subsonic region and thus increases the temperature for $z < z_s$. Consequently, the hydrostatic equilibrium solution for this region is no longer self-consistent; but for most cases of interest, the change in the temperature is unimportant. Similarly, the change in the optical depth scale due to addition of the wind also changes the effective gravity of the photosphere, since $g(z)$ is height-dependent, but our results are only sensitive to changes in gravity of an order of magnitude.

The radiative transfer models depend upon the adopted disk and wind parameters. Observational estimates of the central mass, inner disk radius, and accretion rate in FU Ori are dependent upon the inclination angle, which is only poorly constrained (KHH). We adopt the accretion disk parameters used in our treatment of the near-infrared spectrum of FU Ori (Calvet *et al.* 1991a): $M = 0.49 M_\odot$, $R_i = 4.42 R_\odot$, $\dot{M}_{acc} = 1.59 \times 10^{-4} M_\odot \text{ yr}^{-1}$, except that we take $i = 35^\circ$ rather than $i = 40^\circ$ to provide a slightly better match to rotational velocities. These parameters fix the effective temperature (equation [1]), surface gravity, and the projected rotational velocity of the disk as a function of radius.

The final spectra were computed using a spectral line list kindly provided by R. Kurucz. The g_f values were adjusted to provide agreement between the spectrum of a G supergiant and a non-rotating model atmosphere of appropriate effective temperature and gravity. (We used a G supergiant to provide the best match to the average optical spectrum of FU Ori; see KHH).

In the context of the present simple model, the wind properties are fixed by the parameters \dot{M}_o , a_1 , and Γ . The mass loss parameter \dot{M}_o is constrained by the results of Crowell *et al.* (1987), who estimated a total mass loss rate for the wind $\dot{M}_w \sim 10^{-5} M_\odot \text{ yr}^{-1}$ for FU Ori from modelling the H α and Na I resonance lines. In our final models, we adopt $\dot{M}_o \sim 1 \times 10^{-5} M_\odot \text{ yr}^{-1}$. The other two wind parameters are not as well constrained by other considerations. We adopt $a_1 = 2$, as suggested by the self-similar wind solutions of Blandford & Payne (1982) For this choice, the total mass loss rate from

the disk at radii interior to r is

$$\dot{M}_w(r) = \dot{M}_o \ln(r/R_i). \quad (11)$$

Finally, Γ was adjusted to produce the best agreement with observations. We found that $\Gamma = 1$ results in acceptable line profiles, and is roughly consistent with the velocity law in the standard model of Blandford & Payne (1982).

The wind temperatures of the radiative equilibrium models are in reasonable agreement with the results of Croswell *et al.*, who estimated $T_w \sim 6000$ K for FU Ori; for comparison, at $r = 2R_i$, T_w asymptotically approaches 5420 K. At large distances above the disk, where gas densities are low, there may be departures from radiative equilibrium caused by adiabatic expansion and possible chromospheric heating. We ignore these effects for our initial exploration.

At the innermost disk radius we take to have a wind, $r = 1.36 R_i$, a mass loss rate of $\dot{M}_o = 10^{-5} M_\odot \text{yr}^{-1}$ has a profound effect on the atmospheric structure. Because the continuum opacity depends strongly on temperature, even the relatively modest increase in T_{eff} from 6440 K at $2R_i$ to 7190 K at $1.36 R_i$ causes the photosphere, $z(\tau \sim 2/3)$, to move to considerably higher vertical distances. More importantly, the expansion velocity at the photosphere exceeds 10 km s^{-1} . Thus, at this mass loss rate, and with $\Gamma = 1$, *all photospheric lines* formed at this radius will be appreciably blueshifted.

Roughly 60% of the optical spectrum arises from disk annuli between $1.5 R_i$ and $3 R_i$ (KHH), which can be represented adequately by our results for $r = 2 R_i$. The vertical structure at this annular distance begins to depart considerably from the purely static atmosphere when $\tau_{Ross} \lesssim 2 \times 10^{-2}$. The wind velocity, $\gtrsim 30 \text{ km s}^{-1}$, is already a significant fraction of the disk's projected rotational velocity of $\sim 60 \text{ km s}^{-1}$, so lines formed at or above this level will exhibit profiles strongly affected by expansion.

To illustrate the effects of the wind, we consider three spectral lines which have qualitatively different behavior. The Li I 6707 Å line is always double-peaked in spectra of FU Ori (Hartmann *et al.* 1991; Petrov & Herbig 1992; Welty *et al.* 1992). The strong Fe I 4957 Å line is generally not doubled, but roughly parabolic in shape, with little or no velocity shift (cf. Petrov & Herbig 1992; Welty *et al.* 1992). The Fe II 5018 Å line shows appreciable blueshifted absorption in a "shell" feature. We wish to explore whether a wind with a reasonable mass loss rate can explain the differences in behavior among these lines.

The emergent spectrum is the sum of spectra calculated for different annuli with differing rotational velocities and wind velocities. Figure 3 compares the resultant line profiles with observations of FU Ori obtained with the KPNO 4m echelle spectrograph and TI CCD in December of 1988. Further details of the observations and data reduction can be found in Hartmann & Stauffer (1989) and Hartigan *et al.* (1989).

The model predicts that the Li I line in FU Ori should be double-peaked, as observed, because it forms in a deep layer where the dominant motion is Keplerian rotation. We increased the Li abundance to $\log N_{\text{Li}} = 3.6$ (on a scale where $\log N_{\text{H}} = 12$), a factor of two or more increase over typical pre-main sequence abundance estimates, to provide a better match with observations. The calculated equivalent width is still too small, but the Li I line is very temperature-sensitive, and a modest change in the disk effective temperature might substantially improve the agreement with observation.

The Fe II λ 5018 line lies in the blue spectral region, where line blending is extremely important. The effect of the wind is clearly demonstrated by comparison with the model with no mass loss. The wind model exhibits an absorption “dip”, as observed. In our model, this absorption dip is not the result of a “shell” of material at nearly constant velocity (e.g., Herbig 1966), but instead arises from the convolution of rotation with the wind line profile, as described in the previous section.

We note that agreement between theory and observation requires strong Fe II absorption extending to blueshifts of $v_{\text{max}} = 100 \text{ km s}^{-1}$. At this velocity, with $\Gamma = 1$, $z \sim r$, the assumption of plane-parallel geometry breaks down. However, our model clearly predicts that the Fe II line must be very asymmetric, as observed.

The results for the Fe I 4957 Å “line” are complicated to interpret because this feature is actually a blend of several lines. Two strong Fe I lines from the same multiplet are present; the 4957.60 Å line dominates the blend, but the 4957.30 Å line cannot be neglected. The blend causes the profile of the 4957 Å feature to appear only slightly doubled, even in the absence of any wind (Figure 3).

Our final model for the 4957 Å feature, shown in Figure 3 for a mass loss rate of $1 \times 10^{-5} M_{\odot} \text{ yr}^{-1}$, produces a line blend that is not doubled, as observed, but has a larger equivalent width than indicated by the data. We feel that the agreement between theory and observation is reasonable, given the difficulties of modelling the blended spectrum. In particular, if the model continuum were depressed by approximately 10 % by weak line blanketing, the agreement between theory and observations would become much better.

We emphasize that our model results for the 4957 Å feature are the product of several adjustable parameters, such as $\log gf$ values, turbulent velocities, and blends with unidentified features, in addition to the basic model parameters \dot{M}_o and Γ . Thus, our calculations for this region are not definitive. However, the models demonstrate that for plausible wind parameters, the shape of the 4957 Å feature can be affected by mass loss in such a way as to suppress the double-peaked structure, as observed.

Petrov & Herbig (1992) studied the profiles of about 50 reasonably unblended (mostly neutral metallic) absorption lines in the blue spectrum of FU Ori. Many of these lines exhibited two absorption components. Petrov & Herbig showed that the velocity difference between the two absorption components decreases with decreasing

residual line intensity (increasing line strength). In addition, Petrov & Herbig found that the long-wavelength absorption component becomes progressively blueshifted with increasing line strength, while the short-wavelength absorption component stays roughly at the same velocity (their Figure 7).

The wind model qualitatively explains these effects. To show this without laboriously fitting every line blend, we constructed a sequence of line profiles for $\dot{M}_o = 10^{-5} M_\odot \text{ yr}^{-1}$, using the wavelength and excitation parameters of the Fe I 4957.6 Å line, but using different gf values. This should provide a qualitative treatment of the profiles of neutral metallic lines with excitation potentials ~ 2.8 eV (typical of many lines in this spectral region).

In Figure 4 we display this sequence of Fe I profiles for differing gf values. The velocity splitting between the two components decreases as the line strength increases. In addition, the blue absorption minimum remains at nearly the same velocity, ~ -40 to -35 km s^{-1} , while the red absorption minimum moves considerably closer to line center. Both of these effects are qualitatively similar to the results reported by Petrov & Herbig (1992). When the line is very strong, only one absorption minimum is observed, also in agreement with the results of Petrov & Herbig. It is difficult to make these comparisons more quantitative, because small details of the line profiles depend sensitively on line blending, but it appears that the models reproduce the qualitative behavior of the observations.

Spectral observations at infrared wavelengths sample outer, cooler regions of the disk, compared with optical observations (KHH). Thus, mass-loss signatures in the infrared spectrum provide information on the variation of mass outflow with radius. Using cross-correlation analysis, Hartmann & Kenyon (1987a,b) and Kenyon & Hartmann (1989) suggested that the $v'' - v' = 2 - 0$ first overtone absorption band of CO at $2.3 \mu\text{m}$ might be affected by mass loss. We calculated the $2.3 \mu\text{m}$ CO spectrum, using line parameters described in Calvet *et al.* (1991a). We consider the first overtone $v'' - v' = 2 - 0$ and $v'' - v' = 3 - 1$ bands of CO.

The introduction of a wind with $\dot{M}_o \sim 10^{-5} M_\odot \text{ yr}^{-1}$ produces a small asymmetry in the $v'' - v' = 2 - 0$ band. The 4m FTS spectrum of FU Ori is too noisy for individual lines to be compared with the model. We therefore analyzed the average CO line profiles using cross-correlation analysis (cf. Hartmann & Kenyon 1987a,b; KHH). We used model calculations for no wind, $i = 0^\circ$ as the template spectrum for both FU Ori and the wind model.

The cross-correlation results are shown in Figure 5. The model predicts a modest but significant asymmetry of the $v'' - v' = 2 - 0$ cross-correlation, indicating extra blueshifted absorption. This asymmetry is in reasonable agreement with the cross-correlation of the observed spectrum. The agreement with observations of the $v'' - v' = 2 - 0$ band

may be slightly better for $\dot{M}_o = 10^{-5} M_\odot \text{yr}^{-1}$, but it is not clear whether the limited signal-to-noise values of the observations can support such a distinction.

The cross-correlation of the $v'' - v' = 3 - 1$ region in FU Ori is almost perfectly symmetric; the model cross-correlations are only slightly asymmetric, with a larger asymmetry at higher mass loss rates. As Kenyon & Hartmann (1989) suggested, the first excited vibrational state of CO has a lower population than the ground state in the cool wind, and so the wind is more transparent in the $v'' - v' = 3 - 1$ band.

We find that mass loss rates $\dot{M}_o \lesssim 10^{-6} M_\odot \text{yr}^{-1}$ do not provide any measurable line asymmetry in the $v'' - v' = 2 - 0$ band. The reason for the discrepancy between our results and the estimate $\dot{M}_w \sim 10^{-7} M_\odot \text{yr}^{-1}$ of Kenyon & Hartmann (1989) is that the latter failed to take the distribution of CO molecules over many rotational levels into account.

The model calculations for the near-infrared CO lines are consistent with the wind parameters $\dot{M}_o = 5 \times 10^{-6} - 1 \times 10^{-5} M_\odot \text{yr}^{-1}$, $a_1 = 2$, $\Gamma = 1$, that is, roughly the same parameters as were used to fit the optical lines. However, it should be emphasized that the observational indications of mass loss in the CO first overtone lines are marginal, and that we cannot rule out the possibility that the asymmetry of the $v'' - v' = 2 - 0$ band arises from absorption in a distant, cold, low-density circumstellar shell, rather than a disk wind (see discussion in Kenyon & Hartmann 1989).

Our results suggest that the outflow of FU Ori originates over a substantial area of the inner accretion disk, but not over many decades in radius as suggested by the Pudritz & Norman and Königl models. If dust is not destroyed at temperatures cooler than $\lesssim 10^3$ K, a massive wind produces unacceptably large extinction and infrared excess. This implies that the mass loss rate falls off much faster with radius than in the self-similar model beyond about $12 R_i$. If the blueshifted absorption in the $v'' - v' = 2 - 0$ CO lines arises in a distant circumstellar shell rather than a wind, significant mass loss is limited to a region of several R_i near the central star.

Estimates of mass loss rates depend upon the choice of velocity gradient. We have not been able to reproduce the FU Ori observations with velocity gradients $\Gamma \sim$ unity for $\dot{M}_o = 10^{-6} M_\odot \text{yr}^{-1}$. Conversely, the mass loss from the optical region of the disk cannot be as large as $10^{-4} M_\odot \text{yr}^{-1}$, because then the wind would be optically thick in the continuum. In this case ALL of the absorption lines would be blueshifted by tens of km s^{-1} , whereas the FU Ori objects are all within a few km s^{-1} of the neighboring interstellar medium (Herbig 1966, 1977; Hartmann & Kenyon 1987a,b). Thus, our results reinforce the estimate of $\dot{M}_w \sim 10^{-5} M_\odot \text{yr}^{-1}$ found by Croswell *et al.* (1987) from a study of the H α and Na I line profiles.

The ratio of the kinetic energy loss in the wind L_w to the accretion energy is

$$L_w/L_{acc} = (\dot{M}_w V_w^2 / 2L_{acc}). \quad (14)$$

Our estimates of $\dot{M}_w \sim 10^{-5} M_\odot \text{ yr}^{-1}$ and a terminal wind velocity $V_w \sim 300 \text{ km s}^{-1}$ imply $L_w \sim 0.3 L_{acc}$. This result is an order of magnitude estimate, but it does suggest that the wind may be an important component of the energy budget of the inner disk.

The ratio of wind angular momentum loss to the angular momentum transfer required for steady accretion at \dot{M}_{acc} is more difficult to estimate. Averaged over the inner disk, this ratio is

$$j_w/j_{acc} \sim (\dot{M}_w/\dot{M}_{acc})(\Omega r_A^2/\Omega_K r^2), \quad (15)$$

where r_A is the Alfvén radius of the wind and Ω_K is an average Keplerian angular velocity in the inner disk. If we take $\Omega r_A \sim V_w$ and $\Omega \sim \Omega_K$ (Pudritz & Norman 1986), $\dot{M}_w \sim 10^{-1} \dot{M}_{acc}$, and $\Omega_K r \sim 100 \text{ km s}^{-1}$, the results suggest that the wind may carry away an appreciable fraction of the inner disk angular momentum. However, the limits on mass loss at large radii discussed above indicate that the wind is very unlikely to carry away most of the angular momentum from the *outer* disk.

If the self-similar scaling holds to the smallest radii, we find that the wind from the innermost disk regions is optically thick in the continuum. This material would help to absorb or “hide” any “boundary layer” emission from the inner edge of the disk. In simple disk models, the boundary layer is the narrow disk region where material in Keplerian rotation loses enough energy to come to rest on the slowly-rotating star (Lynden-Bell and Pringle 1974). It is interesting to speculate whether the absorption of boundary layer emission in a optically-thick wind over an area $\sim R_i^2$ could account for the non-detection of boundary layer radiation from FU Ori objects (Kenyon *et al.* 1990).

REFERENCES

- Adams, F.C., Lada, C.J., & Shu, F.H. 1987, *Astrophys. J.* **312**, 788. .
 Basri, G., & Bertout, C. 1989, *Astrophys. J.* **341**, 340.
 Bastian U., & Mundt, R. 1985, *Astron. Astrophys.* **144**, 57.
 Bertout, C., Basri, G., & Bouvier, J. 1988, *Astrophys. J.* **330**, 350.
 Blandford, R.D., & Payne, D.G. 1982, *Mon. Not. Roy. Astron. Soc.* **199**, 883.
 Calvet, N., Patiño, A., Magris C., G., & D’Alessio, P. 1991a, *Astrophys. J.* **380**, 617.
 Calvet, N., Hartmann, L., and Kenyon, S.J. 1991b, *Astrophys. J.* **383**, 752.
 Cassen, P. and Moosman, A. 1981, *Icarus*, **48**, 353.
 Clarke, C. J., Lin, D. N. C., & Pringle, J. E. 1990, *Mon. Not. Roy. Astron. Soc.* **242**, 439.
 Crowell, K., Hartmann, L., & Avrett, E.H. 1987, *Astrophys. J.* **312**, 227.
 Draper, P. W., Warren-Smith, R. F., and Scarrott, S. M. 1985, *Mon. Not. Roy. Astron. Soc.* **212**, 1P.

- Edwards, S., Ray, T.P., & Mundt, R. 1991, in *Protostars and Planets III*, eds. E.H. Levy & M.S. Mathews, in press.
- Gledhill, T. M. and Scarrott, S. M. 1989, *Mon. Not. Roy. Astron. Soc.* **236**, 139.
- Hartigan, P., Hartmann, L., Kenyon, S., Hewett, R., & Stauffer, J. 1989, *Astrophys. J. Suppl.* **70**, 899.
- Hartmann, L., & Kenyon, S.J. 1985, *Astrophys. J.* **299**, 462.
- . 1987a, *Astrophys. J.* **312**, 243.
- . 1987b, *Astrophys. J.* **322**, 393.
- Hartmann, L., & MacGregor, K.B. 1982, *Astrophys. J.* **259**, 180.
- Hartmann, L., Kenyon, S.J., & Hartigan, P. 1991, in *Protostars and Planets III*, eds. E.H. Levy & M.S. Mathews, in press.
- Hartmann, L., & Stauffer, J.R. 1989, *Astron. J.* **97**, 873.
- Herbig, G.H. 1966, in *Vistas in Astronomy*, Vol. 8, eds. A. Beer & K. Aa. Strand (Oxford:Pergamon), p. 109.
- Herbig, G.H. 1977, *Astrophys. J.* **217**, 693.
- Kenyon, S.J., & Hartmann, L. 1987, *Astrophys. J.* **323**, 714.
- . 1989, *Astrophys. J.* **342**, 1134.
- Kenyon, S.J., Hartmann, L., Imhoff, C.L., & Cassatella, A. 1989, *Astrophys. J.* **344**, 925.
- Kenyon, S.J., Hartmann, L.W., Strom, K.M., & Strom, S.E. 1990, *Astron. J.* **99**, 869.
- Kenyon, S. J., Hartmann, L. W., & Hewett, R. 1988, *Astrophys. J.* **325**, 231.
- Königl, A. 1989. *Astrophys. J.* **342**, 208.
- Lada, C.J. 1985, *Ann. Rev. Astron. Ap.* **23**, 267.
- Lovelace, R.V.E., Wang, J.C.L., & Sulkanen, M.E. 1987, *Astrophys. J.* **315**, 504.
- Lynden-Bell, D., & Pringle, J. E. 1974, *Mon. Not. Roy. Astron. Soc.* **168**, 603.
- Monin, J. L., Pudritz, R. E., Rouan, D., and Lacombe, F. 1989, *Astron. Astrophys.* **215**, L1.
- Pelletier, G., & Pudritz, R.E. 1991, preprint.
- Petrov, P.P., & Herbig, G.H. 1992, submitted to *Ap. J.*
- Pringle, J.E. 1989, *Mon. Not. Roy. Astron. Soc.* **236**, 107.
- Pudritz, R.E., & Norman, C.A. 1983, *Astrophys. J.* **274**, 677.
- . 1986, *Astrophys. J.* **301**, 571.
- Reipurth, B. 1989, *Nature*, **340**, 42.
- Reipurth, B. 1990, in *IAU Symposium 137, Flare Stars in Star Clusters, Associations, and the Solar Vicinity*, eds. L.V. Mirzoyan, B.R. Petterson, & M.K. Tsvetkov (Dordrecht: Reidel), p. 229.
- Ruden, S.P., Glassgold, A.E., & Shu, F.H. 1990, *Astrophys. J.* **361**, 546.
- Scarrott, S. M., Draper, P. W., and Warren-Smith, R. F. 1989, *Mon. Not. Roy. Astron. Soc.* **237**, 621.
- Shakura, N. I., & Sunyaev, R. A. 1973, *Astron. Astrophys.* **24**, 337.
- Shu, F.H., Lizano, S., & Adams, F.C. 1987, *Ann. Rev. Astron. Ap.* **25**, 23.

- Shu, F.H., Lizano, S., Ruden, S.P., & Najita, J. 1988, *Astrophys. J. Lett.* **328**, L19.
- Strom, S. E., Strom, K. M., Grasdalen, G. L., Capps, R. W., and Thompson, D. 1985, *Astron. J.* **90**, 2575.
- Terebey, S., Shu, F.H., and Cassen, P. 1984, *Astrophys. J.* **286**, 529.
- Terebey, S., Vogel, S.N., & Myers, P.C. 1989, *Astrophys. J.* **340**, 472.
- Welty, A. *et al.* 1992, in preparation.

Publications

- 1991 "The Dusty Envelopes of FU Orionis Variables", S.J. Kenyon and L.W. Hartmann, *Astrophys. J.* **383**, 664.
- 1991 "FU Orionis Disk Models", L. Hartmann and S.J. Kenyon, in *IAU Colloquium 129, Structure and Emission Properties of Accretion Disks*, eds. C. Bertout, S. Collin-Souffrin, J.P. Lasota, and J. Tran Than Van, Editions Frontieres, in press.
- 1991 "Episodic Phenomena in Early Stellar Evolution", L. Hartmann, invited review, *NATO ASI on The Formation and Evolution of Stars*, eds. N. Kylafis and C. Lada, in press.
- 1991 "Observational Perspectives", L. Hartmann, invited review, *NATO ASW on Angular Momentum of Low Mass Stars*, ed. S. Catalano, in press.
- 1992 "Winds From T Tauri Stars. II. Balmer Line Profiles for Inner Disk Winds", N. Calvet, L. Hartmann, and R. Hewett, *Astrophys. J.* **386**, 229.
- 1992 "Balmer Line Profiles for Infalling T Tauri Envelopes", N. Calvet and L. Hartmann, *Astrophys. J.* **386**, 239.
- 1992 "Mass Loss from Protostellar Accretion Disks. I. The Accelerating Wind of FU Orionis", N. Calvet, L. Hartmann, and S. J. Kenyon, submitted to *Ap. J.*.
- 1992 "Model Scattering Envelopes of Young Stellar Objects. I. Method and Application to Circumstellar Disks", B. A. Whitney and L. Hartmann, submitted to *Ap. J.*.

Figure Captions

Figure 1 - Images of a flared disk illuminated by a central source, at different inclinations $\mu = \cos \theta$ ($\mu = 0$ for edge-on).

Figure 2 - Scattered light images of a disk+envelope system with polar holes illuminated by a central source, at an inclination of $\mu = 0.6$. The contours increase by factors of 2. The minimum contours for each image are, going from left to right and top to bottom, 0.1 , 2×10^{-2} , 1×10^{-3} , 5×10^{-4} , 5×10^{-4} , 1×10^{-4} .

Figure 3 - The profiles of three typical lines, Li I λ 6707, Fe I λ 4957, and Fe II λ 5018, over the entire disk, with $\dot{M}_o = 1 \times 10^{-5} M_\odot \text{ yr}^{-1}$ and $i = 35^\circ$, compared with observations of FU Ori.

Figure 4 - A sequence of disk model line profiles for $\dot{M}_o = 10^{-5} M_\odot \text{ yr}^{-1}$, for the wavelength and excitation parameters of the Fe I 4957.6 Å line, but a range of gf values to illustrate the dependence of profile shape on line strength (see text).

Figure 5 - Cross-correlations of selected CO first overtone band regions. The calculated model spectrum without wind and rotation was used as a template both for the wind models and for FU Ori. The top panel is the correlation of the spectral region between $2.291 \mu\text{m}$ and $2.310 \mu\text{m}$, which includes much of the $v'' - v' = 2 - 0$ band away from the bandhead; the lower panel is the correlation of the region between $2.321 \mu\text{m}$ and $2.349 \mu\text{m}$ for the $v'' - v' = 3 - 1$ band.

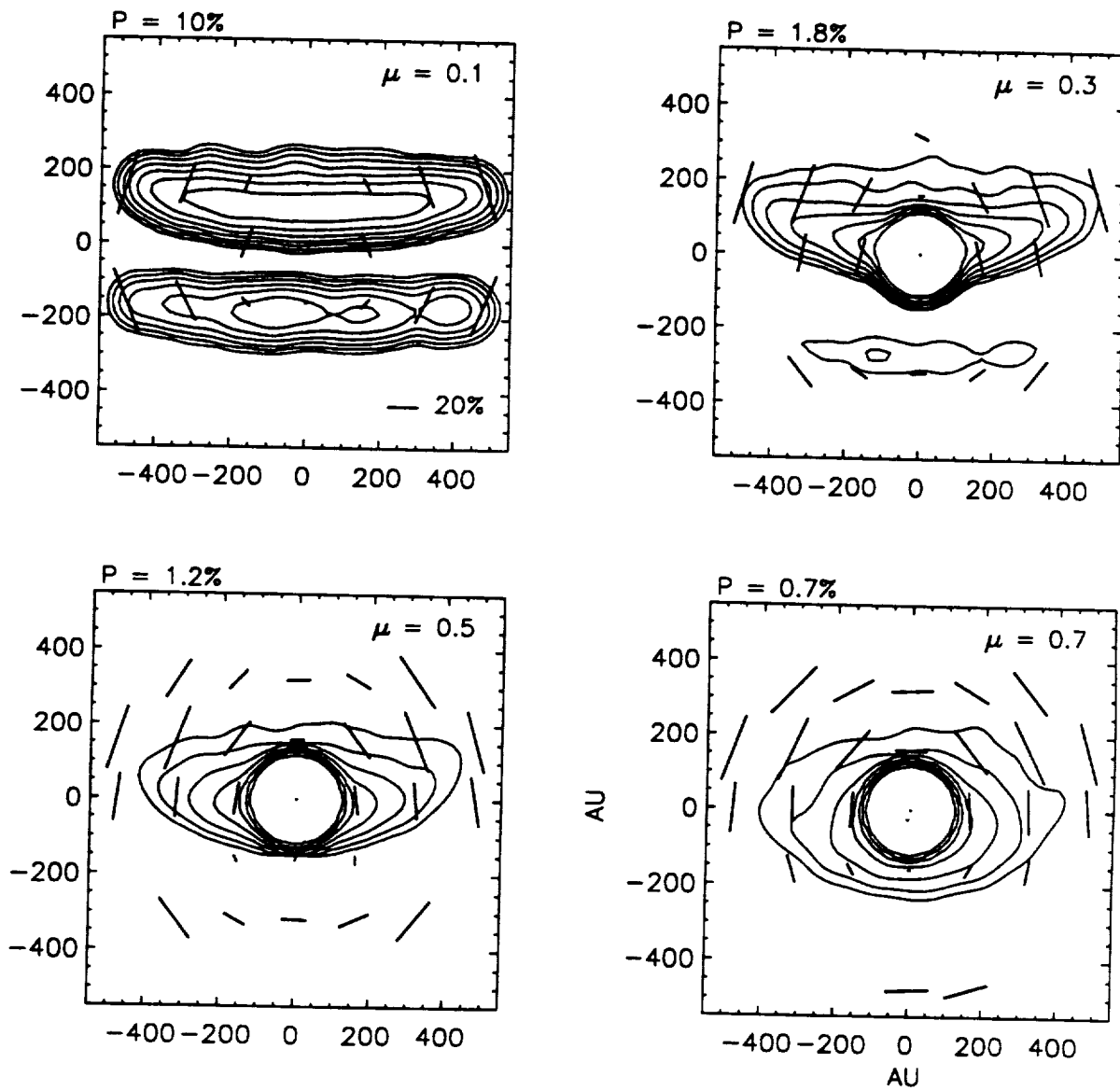


FIGURE 1

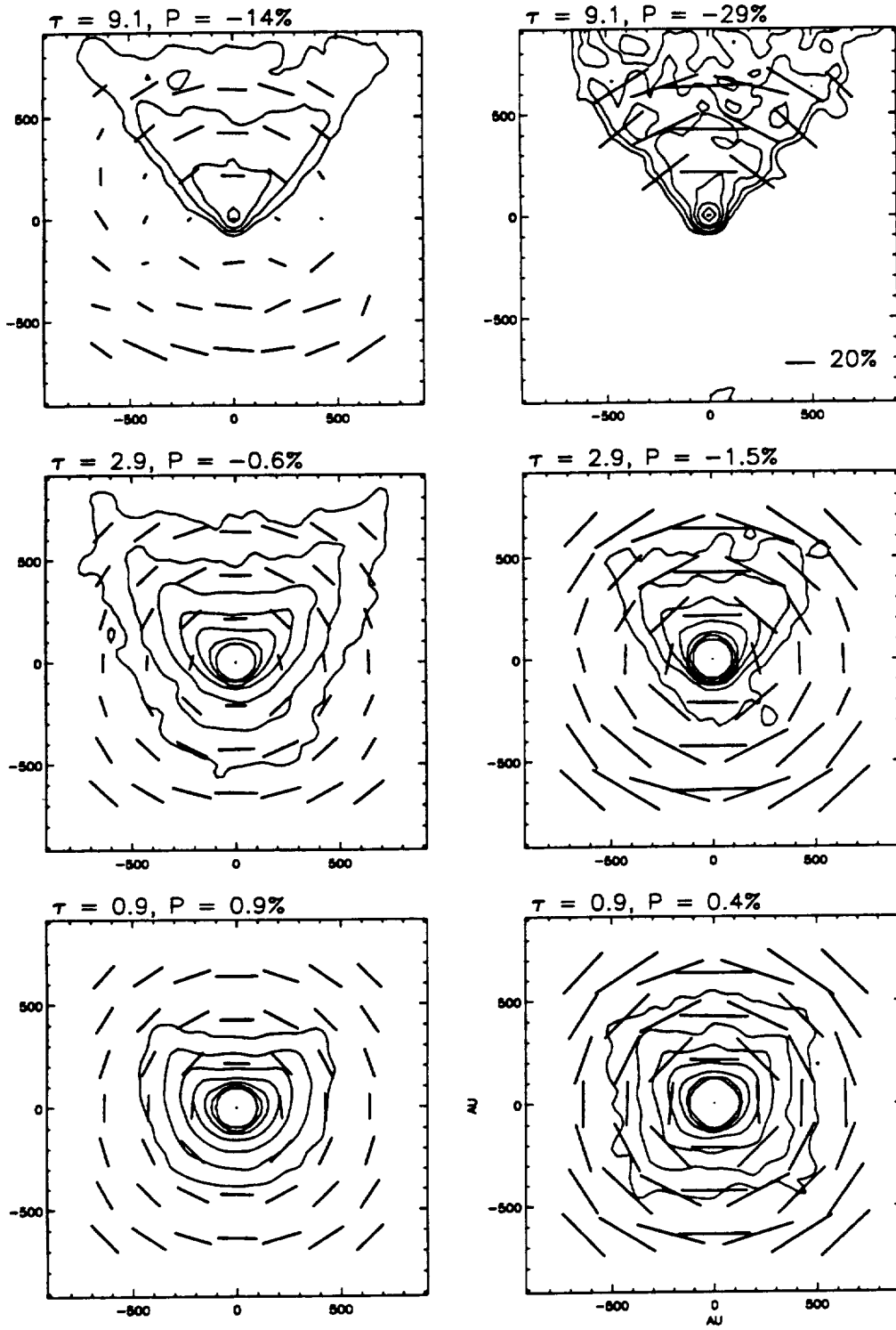


FIGURE 2

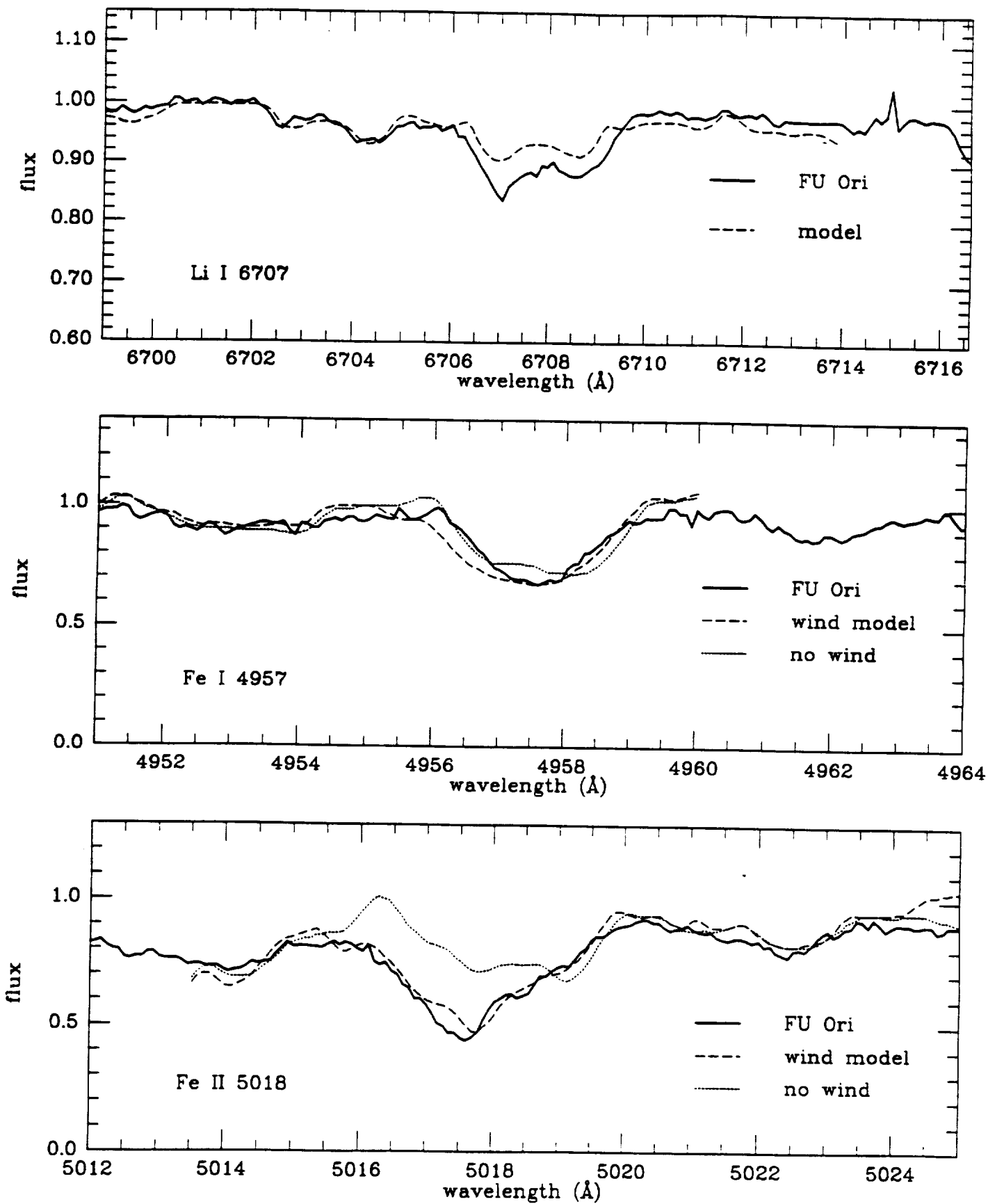


FIGURE 3

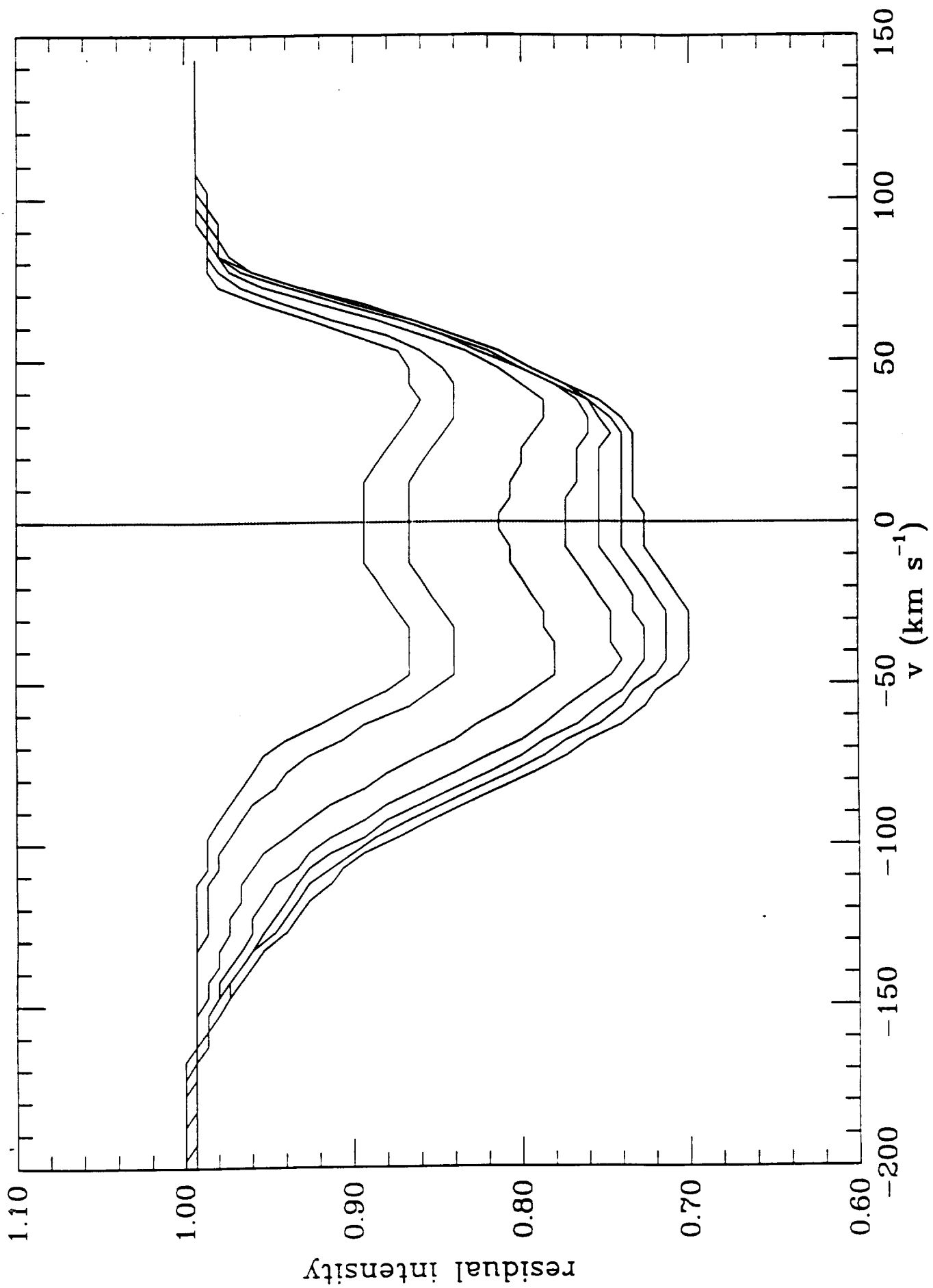


FIGURE 4

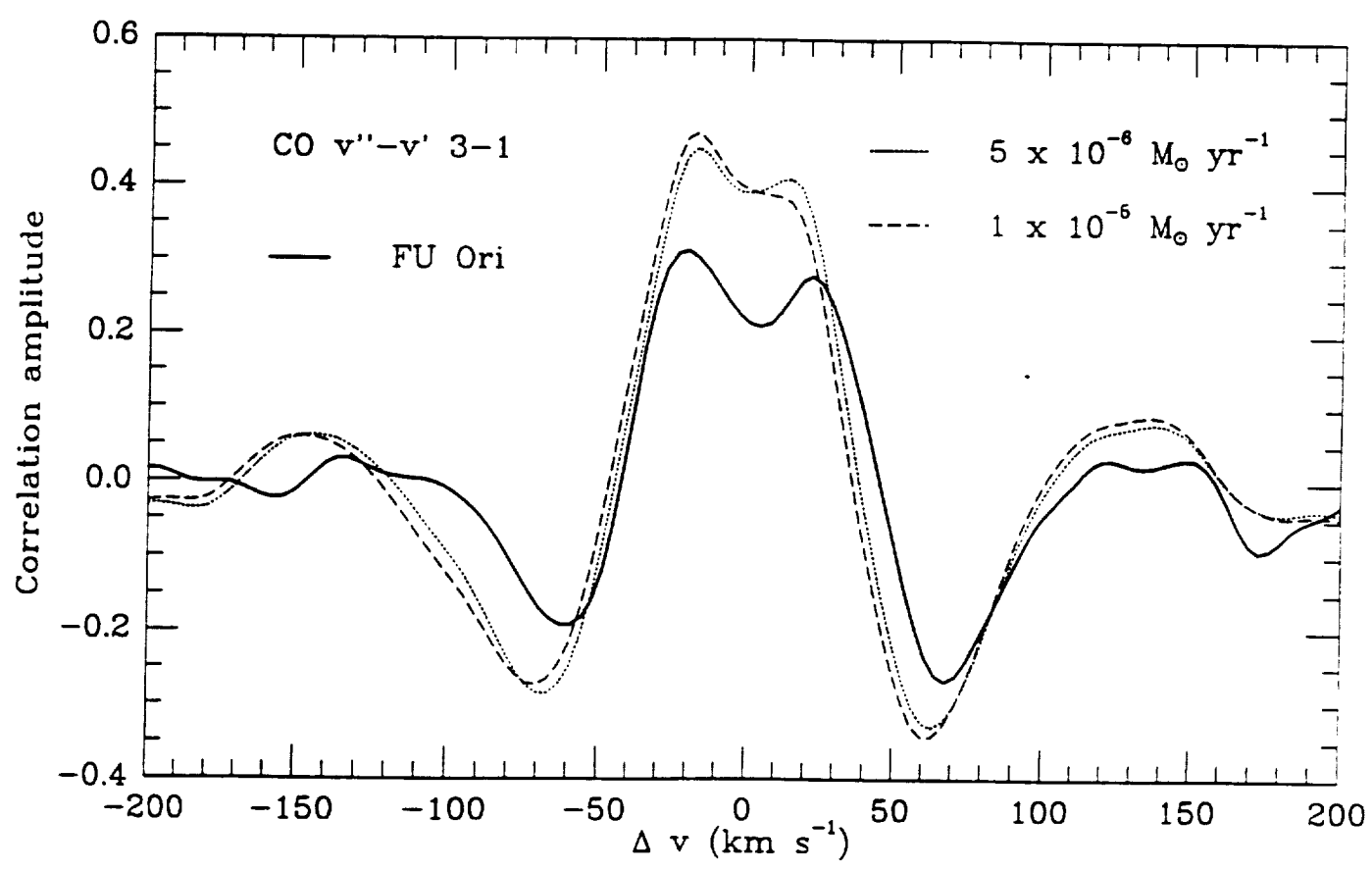
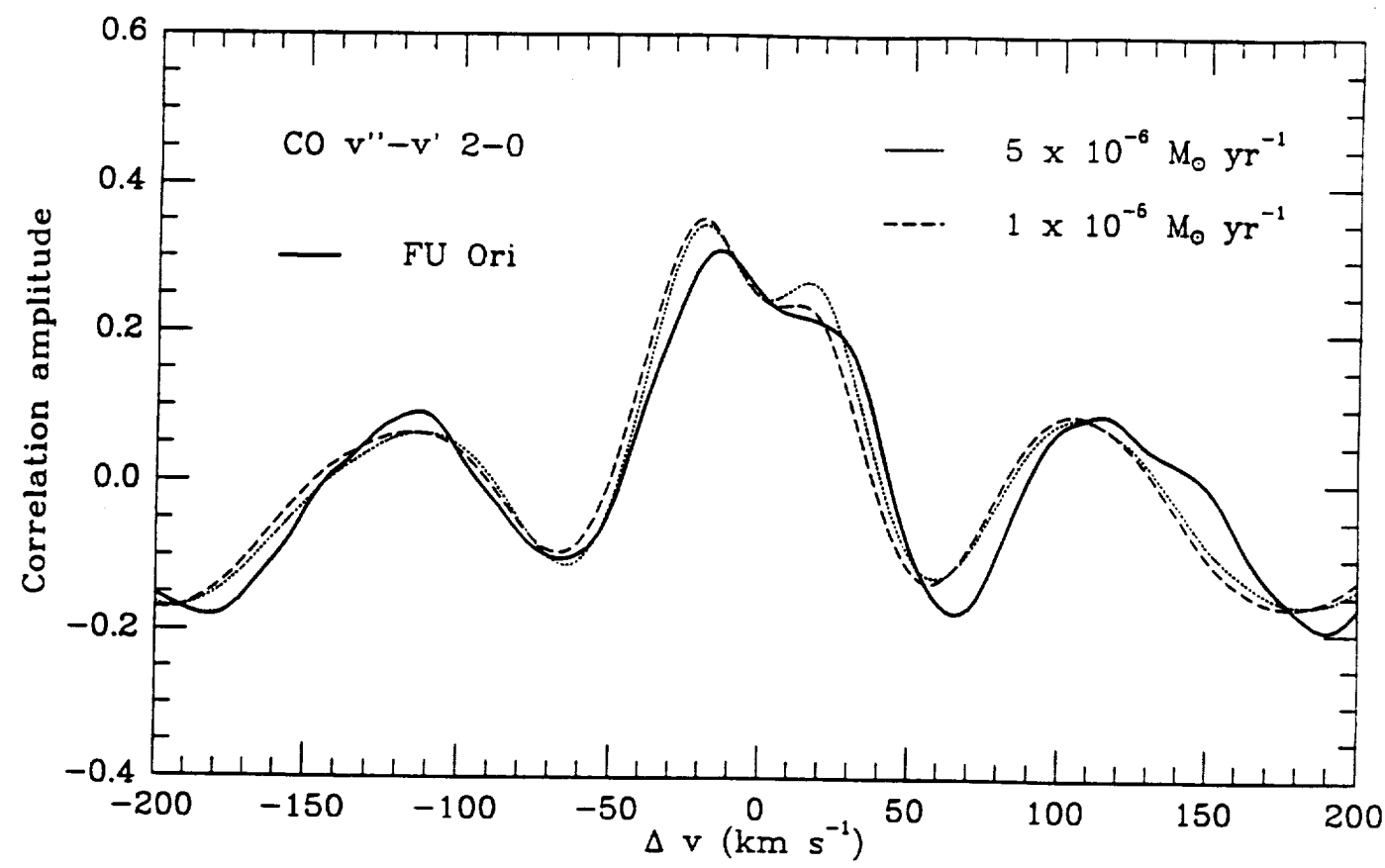


FIGURE 5